Mangler, M.F., Petrone, C.M., and Prytula, J., 2022, Magma recharge patterns control eruption styles and magnitudes at Popocatépetl volcano (Mexico): Geology, https://doi.org/10.1130/G49365.1

Magma recharge patterns control eruption styles and magnitudes at Popocatépetl volcano (Mexico)

Martin F. Mangler[1,2], Chiara Maria Petrone[2], and Julie Prytulak[1]

[1] *Department of Earth Sciences, Durham University, Durham DH1 3LE, UK*

[2] *Department of Earth Science, The Natural History Museum, London SW7 5BD, UK*

SUPPLEMENTAL MATERIALS

Supplemental Material S1 – Full timescale datasets for eruptions of Popocatépetl

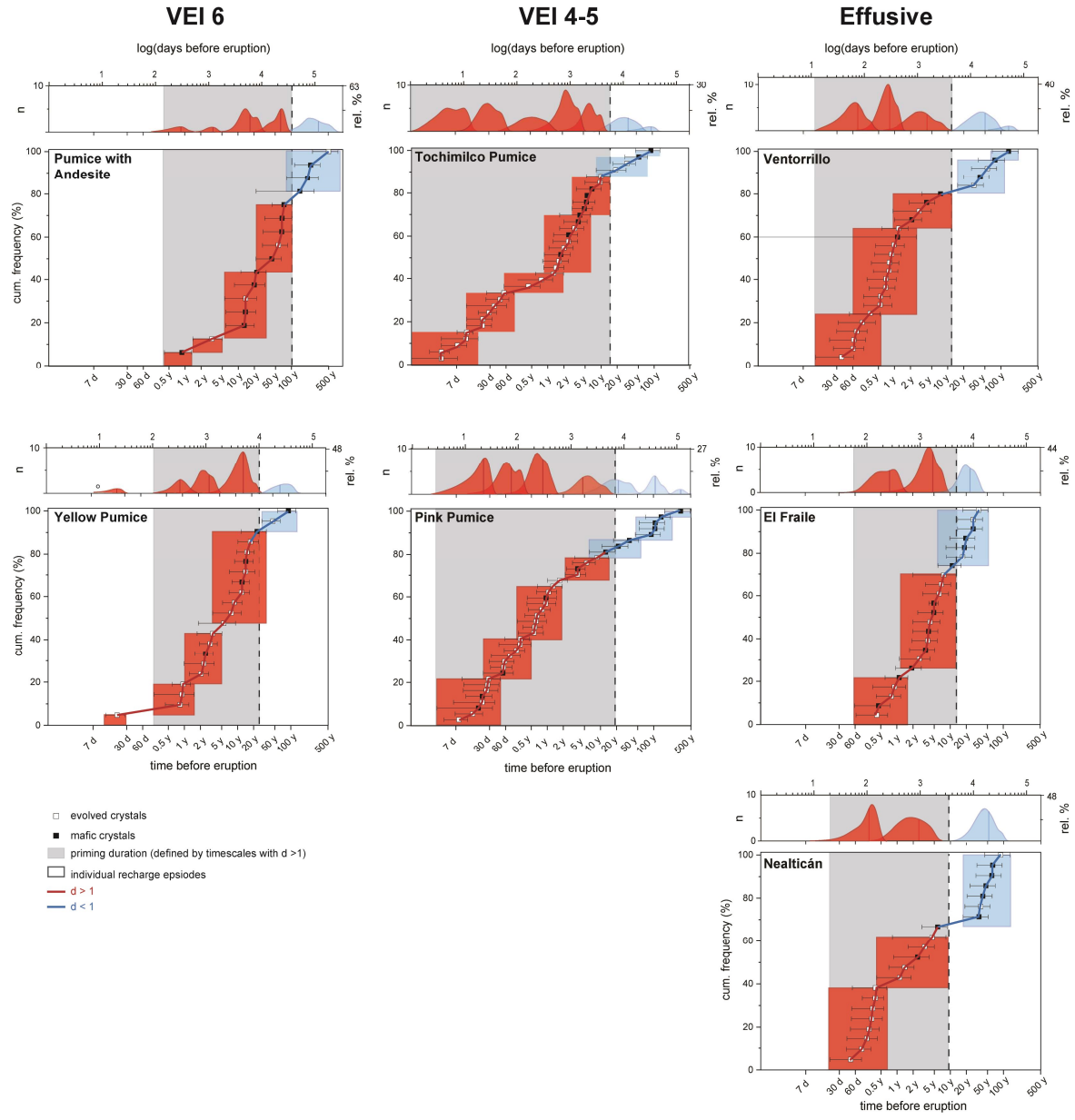

Figure S1.1: *Cumulative frequency plots of Fe-Mg diffusion timescales ± 1SD in orthopyroxene for the seven studied eruptions of Popocatépetl (cf. Figure 2). Grey areas represent priming durations defined by timescale densities d >1. Boxes define individual recharge episodes defined by clusters of timescales with overlapping uncertainties; data are clustered backwards, i.e., starting at the shortest timescale. Recharge episodes forming part of the priming duration are colored red; those preceding the priming period are colored blue. Upper panels show kernel density functions (KDFs) for each episode and form the basis for Figure 3.*

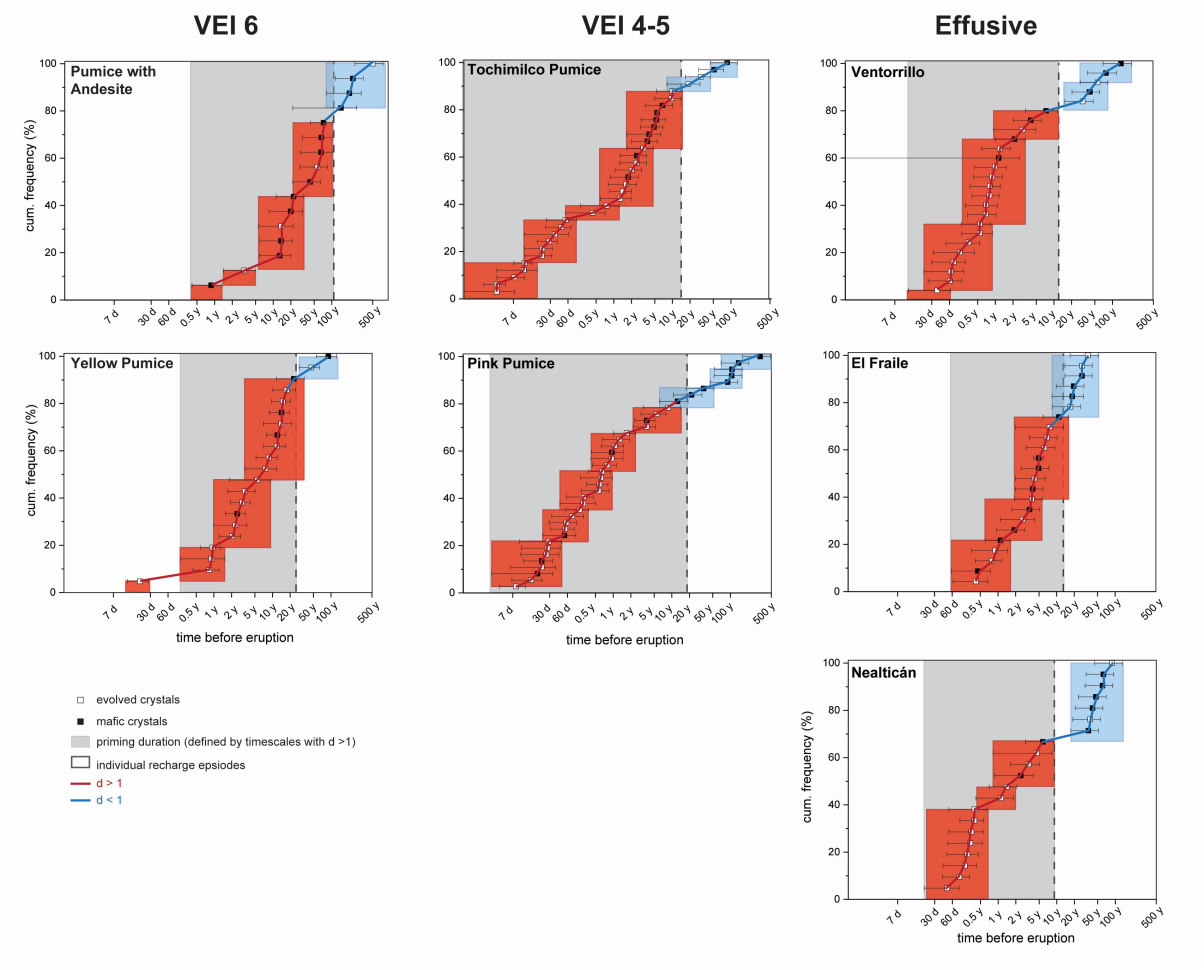

Figure S1.2: *Cumulative frequency plots of Fe-Mg diffusion timescales ± 1SD in orthopyroxene for the seven studied eruptions of Popocatépetl. Timescale data is forward clustered,, i.e., starting at the longest timescales. The resulting number of recharge episodes for each eruption closely matches those derived from backward clustering (Figure S1.1).*

Table S1: *Fe-Mg diffusion data and timescale densities for orthopyroxenes from eruptions of Popocatépetl.* **- See separate Excel Sheet.**

Supplemental Material S2 – Fe-Mg diffusion modeling of Popocatépetl orthopyroxene crystals

2.1 Crystal selection

Orthopyroxene crystals in pumice samples were hand-picked from lightly crushed pyroclasts under a binocular microscope. No systematic variation of textures with crystal size was observed, therefore crystals were picked from the most abundant size fractions, i.e., 125–250 μm, 250–500 μm, and 500–1000 μm. Orthopyroxene crystals in lavas were selected from thin sections directly as they tend to fracture when applying conventional mineral separation techniques. Samples were surveyed using an optical microscope and on the scanning electron microscope, and suitable crystals were selected according to the following criteria (see also Krimer and Costa, 2017):

• Crystal Sections: Crystal sections parallel to the c-axis were targeted to enable modeling along the a- or b-axes. The most accurate diffusion models are produced by ab-sections (Krimer and Costa, 2017), and we chose such crystals whenever possible; however such sections perpendicular to the c-axis are rare. Crystals with oblique sections or asymmetrical diffusion patterns were avoided.

• Textures: Well developed boundaries between compositional zones are required, ideally throughout the crystal, i.e., crystals with discontinuous or invasive boundaries were avoided.

• Boundary and initial conditions: Crystals need to show concentration plateaux on both sides of the compositional profile, and the transition may not be disturbed by growth or dissolution effects. Compositional profiles of trace elements with low diffusion rates (e.g., Al; Cherniak and Dimanov, 2010) were used to confirm initial conditions (i.e., the initial

shape of the profile), and to exclude interfering factors such as growth during differentiation or dissolution (Fig. S2.1).

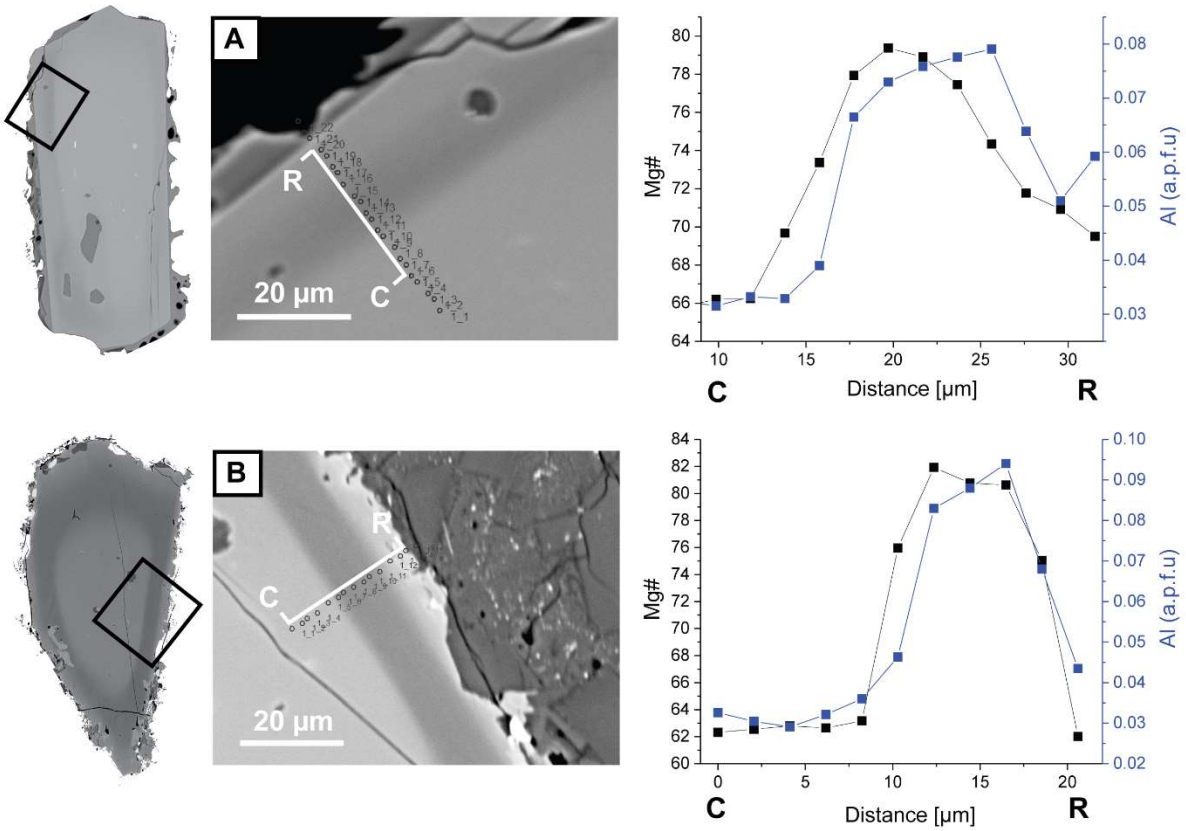

Figure S2.1. *Backscattered electron (BSE) images and compositional transects acquired by electron probe microanalysis (EPMA) showing the variation of Mg# and Al concentrations across zoned orthopyroxene crystals. Aluminium is chosen due to its lower diffusion rate compared to Mg, which can be used to distinguish between growth/dissolution and diffusion, and to identify initial conditions. (A) Banded crystal with diffused Mg# profile. (B) Undiffused, banded crystal with well-defined profiles for Mg# and Al concentrations.*

2.2 Compositional transects

High-resolution backscattered electron (BSE) images of zoned minerals were acquired at the Natural History Museum, London, on a FEI Quanta 650 ESEM field emission gun at 15 kV acceleration voltage, 15 mm working distance, a beam size of 3 – 3.5 and 10 – 30 µs dwell time.

Compositional profiles perpendicular to the c-axis were extracted from BSE greyscale images as they offer a superior spatial resolution (pixel spacing of <0.1 µm) compared to electron microprobe analysis (~2 µm; Fig. S2,2). Grey values from BSE images are strongly correlated with the Mg# of orthopyroxene ($R^2 = 0.9982$) and have been used routinely in previous diffusion modeling studies as a proxy for pyroxene compositions (e.g., Morgan et al., 2004; Allan et al., 2013; Chamberlain et al., 2014; Kilgour et al., 2014; Petrone et al., 2016). Extraction was performed using the greyvalues MATLAB script (Petrone et al., 2016), which calculates greyscales according to the nearest neighbour colour interpolation method. Each data point represents the average ± 2 SE of several hundreds of line measurements (e.g., 327 lines, blue in Fig. S2.2).

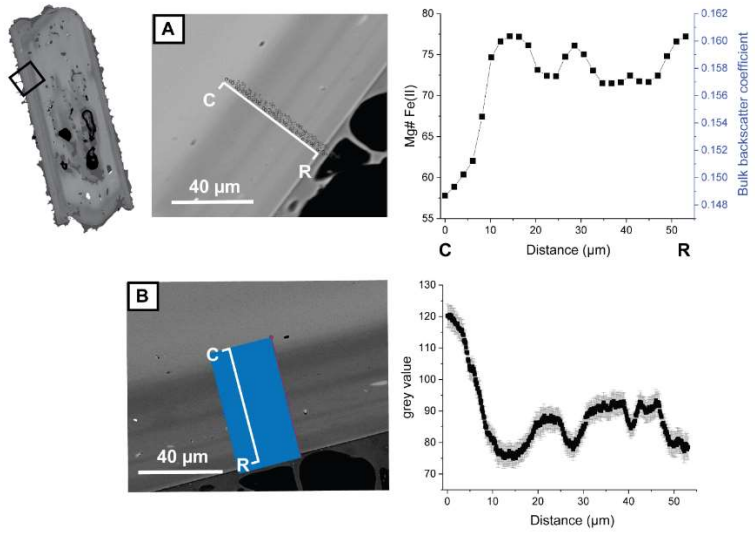

Figure S2.2*. BSE images and compositional profiles of a multiply zoned orthopyroxene crystal. (A) Core – rim profile of Mg# acquired by EPMA. (B) Grey values extracted from high resolution BSE images along the same core – rim transect as in (A). The blue box represents the area the compositional transect is integrated from using the MATLAB script greyvalues (Petrone et al., 2016). Grey values show a strong negative correlation to Mg#, and extracted profiles offer a superior resolution compared to EPMA data*

.

98 ***2.3 Diffusion coefficient***

99 Diffusion timescales reported in this study were calculated using D_{Fe-}^{opx} of Dohmen
100 et al. (2016). Their expression requires temperature and oxygen fugacity as input parameters
101 to calculate specific *D*s, but does not include a correction for pyroxene composition as they
102 report negligible dependency of D_{Fe-Mg}^{opx} on composition of Fs <50. Temperatures were
103 calculated individually for each compositional zone in modeled crystals following the method
104 described in detail in Mangler et al. (2020). For the oxygen fugacity, we used 14 touching
105 ilmenite-magnetite pairs in the Yellow Pumice, Pink Pumice and Nealticán lava satisfying
106 Bacon and Hirschmann (1988)'s equilibrium conditions (Table S2; see separate Excel Sheet).
107 The average oxygen fugacity calculated after Ghiorso and Evans (2008) is ΔNNO = 0.7 (f_{O_2}
108 = $10^{-9.730}$), in agreement with previous estimates for Popocatépetl, ranging from ΔNNO = 0 –
109 1.5 (Schaaf et al., 2005; Witter et al., 2005; Atlas et al., 2006; Sosa-Ceballos et al., 2014).
110 Dohmen et al. (2016) suggest that diffusion perpendicular to the c axis is up to 3.5 times
111 slower than along [001], hence we applied this factor to our results, which therefore represent
112 maximum values.
113
114 ***2.4 Numerical modeling***

115 Diffusion modeling was performed using the MATLAB script createfit (Petrone et al.,
116 2016). Required inputs are the compositional transect as a *.csv file (generated by the
117 *greyvalues* script; Fig. S2.2), and *D* (as ΔH and D_0) for the relevant crystal orientation (here:
118 a-axis), temperature (individual for each modelled boundary), and oxygen fugacity (here: f_{O_2}
119 = $10^{-9.730}$). A non-linear least squares fit to the given compositional profile is iteratively
120 calculated assuming diffusion across a semi-infinite plane sheet (eq. 2.14, Crank, 1979),
121 using

(1)

123 $$y = y_0 + \frac{C_0}{2}\ erf\left(\frac{x - x_0}{\sqrt{4Dt}}\right)$$

122

124 where y is the grey value at point x (μm), and x_0 and y_0 are the coordinates of the flex point
125 of the profile. The *createfit* script performs an error propagation for the errors on the fitting
126 parameter $\sqrt{4Dt}$ and the temperature (Petrone et al., 2016). Depending on data density and
127 the quality of the fit, the error on $\sqrt{4Dt}$ is typically between 5 and 20 % (1SD; Fig. S2.3).
128 Uncertainties on the temperatures used have a more significant effect on the calculated
129 timescales, typically ranging from 40 – 60% for temperature uncertainties of 15 – 30°C.

130

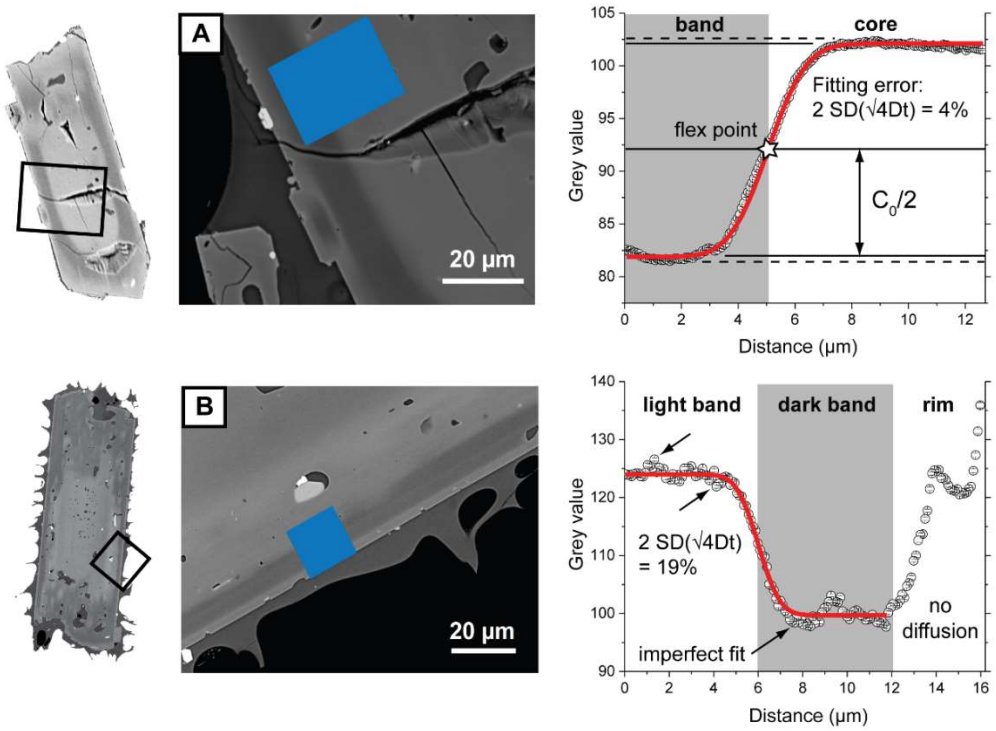

131 ***Figure S2.3.*** *BSE images of banded orthopyroxene crystals, extracted greyscale profiles and fits*
132 *modelled using the MATLAB script createfit (Petrone et al., 2016). The blue box in BSE images*
133 *represents the area the compositional transect is integrated from, using the MATLAB script greyvalues*
134 *(Petrone et al., 2016). (A) Crystal showing a core-band transect with a good fit of the diffusion model*
135 *(red line). (B) Crystal with irregular core-band transition, resulting in an imperfect fit of the diffusion*
136 *model and larger associated errors.*

Pink Pumice

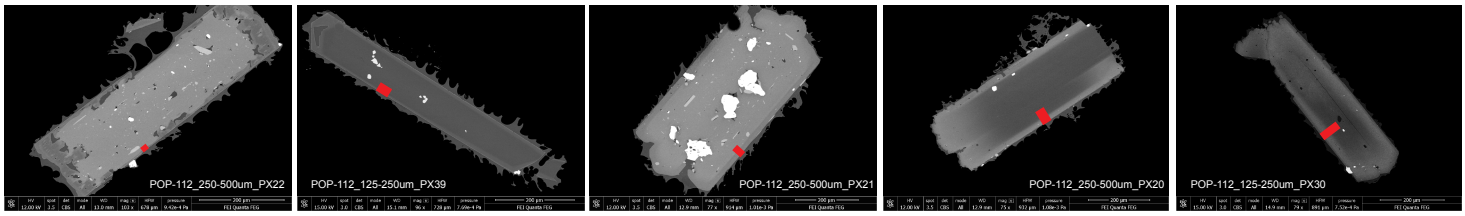

Nealticán

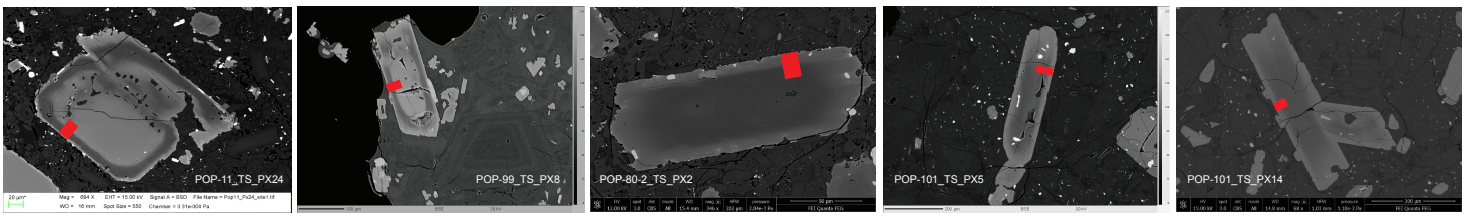

Yellow Pumice

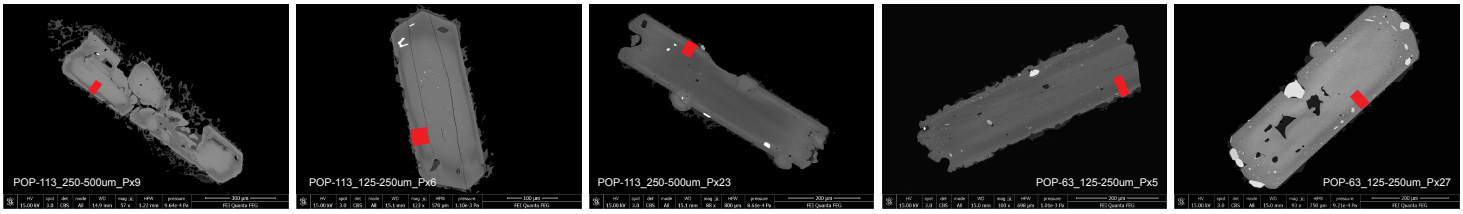

Pumice with Andesite

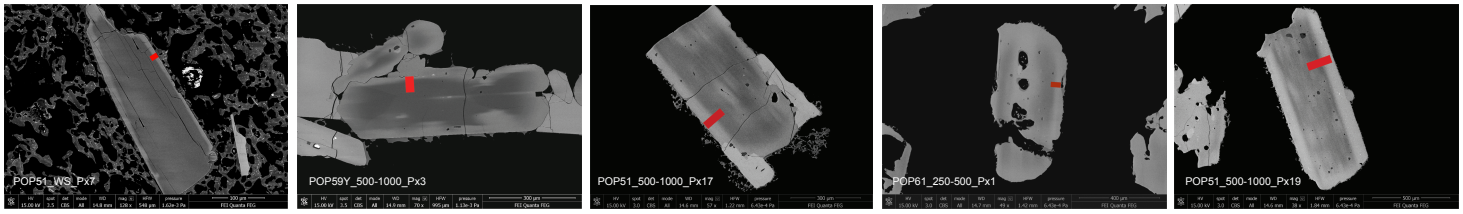

El Fraile

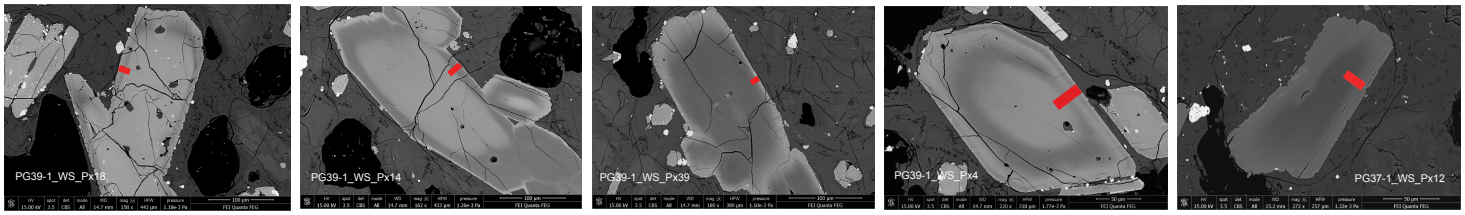

Tochimilco Pumice

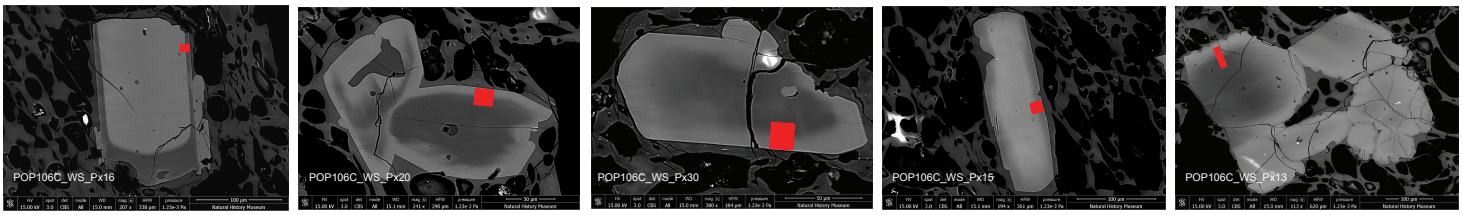

Ventorrillo

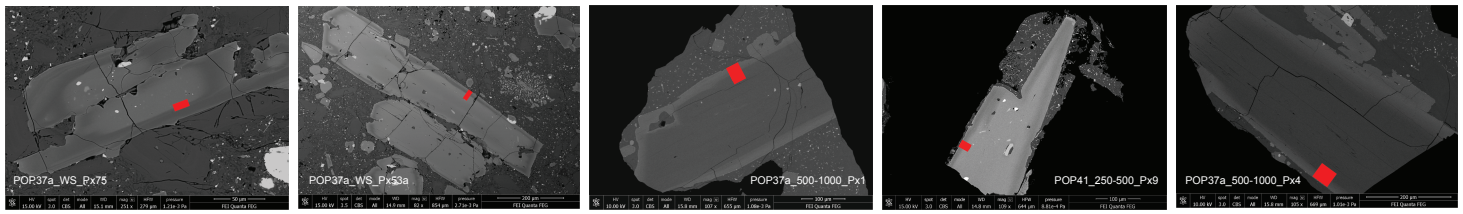

Fig. S2.4*. Representative BSE images of orthopyroxene crystals selected for diffusion modeling in this study. Red boxes outline where the compositional transects for the models were taken.*

Supplemental Material S3 – Priming durations for eruptions with published diffusion data

Table S3: *Compilation of published diffusion timescales and calculated timescales densities to define priming durations.* **- See separate Excel Sheet.**

REFERENCES CITED

Allan, A. S. R., Morgan, D. J., Wilson, C. J. N., and Millet, M.-A., 2013, From mush to eruption in centuries: assembly of the super-sized Oruanui magma body: Contributions to Mineralogy and Petrology, v. 166, no. 1, p. 143-164, doi: 10.1007/s00410-013-0869-2

Atlas, Z. D., Dixon, J. E., Sen, G., Finny, M., and Martin-Del Pozzo, A. L., 2006, Melt inclusions from Volcán Popocatépetl and Volcán de Colima, Mexico: Melt evolution due to vapor-saturated crystallization during ascent: Journal of Volcanology and Geothermal Research, v. 153, no. 3-4, p. 221-240, doi: 10.1016/j.jvolgeores.2005.06.010

Bacon, C. R., and Hirschmann, M. M., 1988, Mg/Mn partitioning as a test for equilibrium between coexisting Fe-Ti oxides: American Mineralogist, v. 73, no. 1-2, p. 57-61

Chamberlain, K. J., Morgan, D. J., and Wilson, C. J. N., 2014, Timescales of mixing and mobilisation in the Bishop Tuff magma body: perspectives from diffusion chronometry: Contributions to Mineralogy and Petrology, v. 168, no. 1, doi: 10.1007/s00410-014-1034-2

Cherniak, D., and Dimanov, A., 2010, Diffusion in pyroxene, mica and amphibole: Reviews in Mineralogy and Geochemistry, v. 72, no. 1, p. 641-690

Crank, J., 1979, The mathematics of diffusion, Oxford university press.

Dohmen, R., Ter Heege, J. H., Becker, H.-W., and Chakraborty, S., 2016, Fe-Mg interdiffusion in orthopyroxene: American Mineralogist, v. 101, no. 10, p. 2210-2221, doi: 10.2138/am-2016-5815

Frost, B. R., 1991, Introduction to oxygen fugacity and its petrologic importance: Reviews in Mineralogy and Geochemistry, v. 25, no. 1, p. 1-9, doi: 10.1515/9781501508684-004

Ghiorso, M. S., and Evans, B. W., 2008, Thermodynamics of rhombohedral oxide solid solutions and a revision of the Fe-Ti two-oxide geothermometer and oxygen-barometer: American Journal of science, v. 308, no. 9, p. 957-1039, doi: 10.2475/09.2008.01

Kilgour, G. N., Saunders, K. E., Blundy, J. D., Cashman, K. V., Scott, B. J., and Miller, C. A., 2014, Timescales of magmatic processes at Ruapehu volcano from diffusion chronometry and their comparison to monitoring data: Journal of Volcanology and Geothermal Research, v. 288, p. 62-75, doi: 10.1016/j.jvolgeores.2014.09.010

Krimer, D., and Costa, F., 2017, Evaluation of the effects of 3d diffusion, crystal geometry, and initial conditions on retrieved time-scales from Fe–Mg zoning in natural oriented orthopyroxene crystals: Geochimica et Cosmochimica Acta, v. 196, p. 271-288, doi: 10.1016/j.gca.2016.09.037

Morgan, D. J., Blake, S., Rogers, N. W., DeVivo, B., Rolandi, G., Macdonald, R., and Hawkesworth, C. J., 2004, Time scales of crystal residence and magma chamber volume from modelling of diffusion profiles in phenocrysts: Vesuvius 1944: Earth and Planetary Science Letters, v. 222, no. 3-4, p. 933-946, doi: 10.1016/j.epsl.2004.03.030

Petrone, C. M., Bugatti, G., Braschi, E., and Tommasini, S., 2016, Pre-eruptive magmatic processes re-timed using a non-isothermal approach to magma chamber dynamics: Nature communications, v. 7, no. 12946, doi: 10.1038/ncomms12946